ELSEVIER

International Journal of Adhesion & Adhesives 27 (2007) 679–686

International Journal of Adhesion & Adhesives

www.elsevier.com/locate/ijadhadh

Strength of epoxy adhesive-bonded stainless-steel joints

A.B. de Morais*, A.B. Pereira, J.P. Teixeira, N.C. Cavaleiro

[a]*University of Aveiro, Department of Mechanical Engineering, Campus Santiago, 3810-193 Aveiro, Portugal*

Accepted 14 February 2007
Available online 3 March 2007

Abstract

The strength of stainless-steel joints bonded with two epoxy adhesives was investigated. The experimental programme included tests on single-lap and butt joints, as well as thick-adherend and napkin ring shear tests. Results suggested that the tensile and shear strengths of the epoxy adhesives were quite similar. However, finite element (FE) analyses raised doubts on the true adhesive strengths, due to the complex stress state in joint tests and pressure-dependent adhesive behaviour. In spite of some uncertainties, FE analyses showed that failure could be fairly well predicted by a maximum shear strain criterion.

Keywords: Lap-shear; Butt joints; Finite element stress analysis; Joint strength

1. Introduction

Adhesive joints are finding increasing structural applications in various fields, especially for high performance composites. However, designers still face important difficulties associated to the lack of well-established failure criteria. Although a few analytical solutions [1,2] for lap joints remain a reference for researchers and designers, it has become clear that only finite element (FE) models are able to handle the complexities of joint strength prediction [3]. In fact, failure of adhesive joints usually involves considerable geometrical and material non-linearity. Moreover, even the presence of spew fillets seems to affect significantly joint strength [3–5]. However, it is unlikely that future design methods rely on such a feature. On the other hand, adopting the simple sharp edge geometry gives rise to stress singularities at the adherend/adhesive interface [6,7]. Approaches that overcome the singularity problem have been proposed i.e. design based on stresses at characteristic distances from the edge or assuming rounded adherend corners [7]. However, these methods introduce additional empirical parameters and thus are unlikely to gain acceptance.

Fracture mechanics has been proposed as a more suitable approach to predict the strength of adhesive joints [8,9]. Recently, fracture mechanics crack based crack propagation criteria have been combined with stress-based crack initiation criteria in cohesive zone models [10–13]. These models are implemented in interface finite elements and can often be used to model the adhesive layer across the whole thickness [10–12]. Alternatively, zero-thickness interface elements can be placed along the interface and/or inside the adhesive layer [13]. In spite of the enormous potential, cohesive zone models have not yet found extensive experimental support. Moreover, it has been difficult to evaluate local failure mechanisms, because of large-scale deformations of the adhesive layer, adherend plasticity and high influence of joint geometry [12]. Nevertheless, numerical analyses performed by Campilho et al. [13] indicated that joint failure is actually dictated by adhesive strengths and little dependent on fracture toughness. This seems to agree with the experimental study by Pereira and Morais [14], which concluded that the strength of adhesive joints was practically insensitive to the presence of end cracks.

In view of the current state-of-the-art, an experimental study was conducted on various types of stainless-steel joints bonded with two epoxy adhesives. FE analyses were subsequently performed in order to identify a joint failure criterion.

*Corresponding author. Tel.: 351 234 370830; fax: 351 234 370953.
E-mail address: abm@mec.ua.pt (A.B. de Morais).

0143-7496/$ - see front matter © 2007 Elsevier Ltd. All rights reserved.
doi:10.1016/j.ijadhadh.2007.02.002

2. Experimental

2.1. Procedures

Rolled AISI 304 stainless-steel adherends were used in all joints tested. Besides having chemically stable surfaces, the plastic stress–strain behaviour of this material has been studied in detail [15]. The joints were prepared with two adhesives:

- Araldite Standard (AS), a two-part epoxy from Ciba, which was subjected to a curing cycle of 3 h at 80 °C;
- L3450, a room temperature cure two-part epoxy from Loctite.

Adherend surfaces were manually abraded with emery paper (220 grade), cleaned and degreased with acetone. Auxiliary rigs, spacers and weights were used during bonding to ensure accurate alignment and a uniform 0.22 mm layer thickness. A limited set of tests was performed on joints with spew fillets. In general, however, adhesive filets were carefully removed with a knife while lightly compressing the overlap area of the specimen. Optical microscope observations were made to detect possible damage near the edges and to check the adhesive layer thickness.

The experimental programme included:

- butt joint tensile (BJT) tests, using $D = 20$ and 30 mm diameter bars;
- napkin ring shear (NRS) tests in accordance with the former ASTM E229-97 standard;
- lap-shear tests on single-lap joints (SLJ) (Fig. 1) with $b = 25$ mm width, adherend thickness $t = 1.5$, 3.0 and 5.0 mm and overlap length $L = 12.5$, 25 and 40 mm. They are designated in the SLJ (t,L) format;
- thick-adherend shear (TAS) tests (Fig. 2), similar to those of ISO 11003-2 standard [16], on joints with $L = 10$, 20, 30 and 40 mm and $b = 25$ mm width. Designation format is TAS(L).

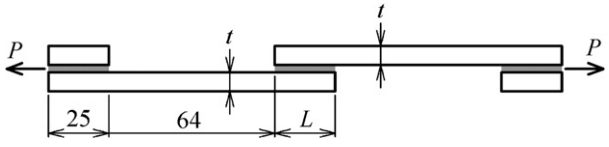

Fig. 1. Geometry (mm) of single-lap joints (SLJ) tested.

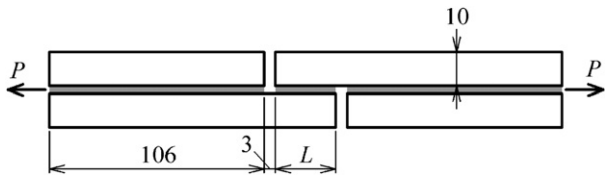

Fig. 2. Geometry (mm) of thick-adherend shear (TAS) joints tested.

All tests were carried out in a Shimadzu 50 kN-AG machine on a minimum of five specimens of each joint type. In BJT and NRS tests, tensile $\sigma_u = 4P_u/\pi D^2$ and shear $\tau_u = 16P_uD/\pi(D^4–d^4)$ strengths were calculated from failure loads P_u, D and d designating the outer and inner joint diameter. Results of the other tests were expressed by an apparent shear strength $\tau_{ua} = P_u/bL$. In the case of the TAS(10) test, τ_{ua} is considered practically equal to the adhesive shear strength τ_u, since the small overlap provides an approximately uniform shear stress distribution.

2.2. Results and discussion

As in [14], all joints bonded with AS failed adhesively, while the ones bonded with L3450 failed cohesively. Fig. 3 summarises strength results of BJT, NRS and TAS(10) tests in terms of average values (columns) and scatter interval (error bars). It can be seen that NRS and TAS(10) tests gave very similar shear strengths for both adhesives. On the other hand, tensile strengths were not significantly dependent on butt joint diameter, which suggests that alignment was adequate in the tests. Moreover, tensile strengths were very close to shear strengths. There is indeed some evidence [17,18] that polymers have similar tensile and shear strengths and actually undergo tensile failure in shear tests. However, it is well known that the suitability of BJT tests for measuring adhesive tensile strengths is highly questioned [3], due to significant radial stresses and edge effects. Silva and Adams [19] have recently performed tensile tests on bulk specimens and TAS tests for various adhesives at different temperatures. They obtained shear-to-tensile strength ratios from 0.72 to 0.83 at room temperature, thus above the von Mises 0.58 ratio. However, it is questionable that bulk specimens represent adequately thin adhesive layers, as size effects on strengths [7] and failure strains [20] have been detected. Clearly, many uncertainties remain on the multiaxial stress–strain behaviour of adhesives.

Figs. 4–7 present measured SLJ apparent strengths. It can be seen that τ_{ua} values decreased for increasing overlap lengths L, a trend that can be easily explained by increasing

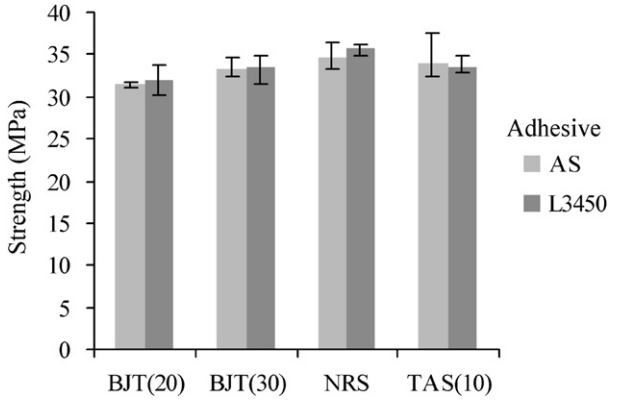

Fig. 3. Average and scatter interval of strengths measured in BJT (20 and 30 mm diameter specimens), NRS and 10 mm overlap TAS tests.

stress concentration at joint ends (see Section 3.2). However, joint failure loads increased with L. Figs. 4–7 also show that τ_{ua} increased with adherend thickness. In fact, the higher bending stiffness of the adherends reduces stress concentration (see Section 3.2). On the other hand, the removal of spew fillets did not introduce additional scatter, but reduced joint strengths (Figs. 8 and 9). In general, the effect of spew fillet removal increased with L. Again, this can be explained by increasing stress concentration at joint ends, which is reduced by the presence of

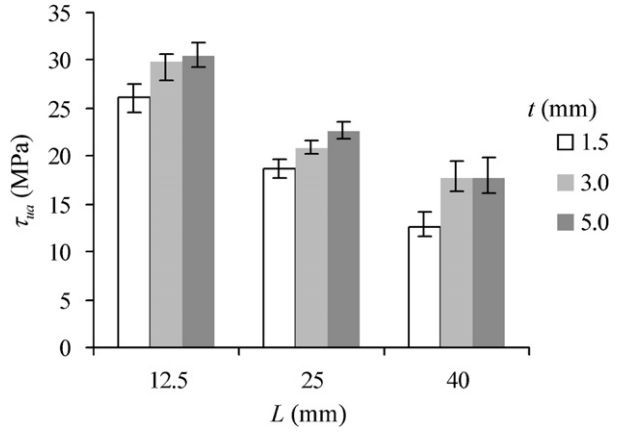

Fig. 4. Average and scatter interval of apparent strengths measured for AS SLJ with spew fillets.

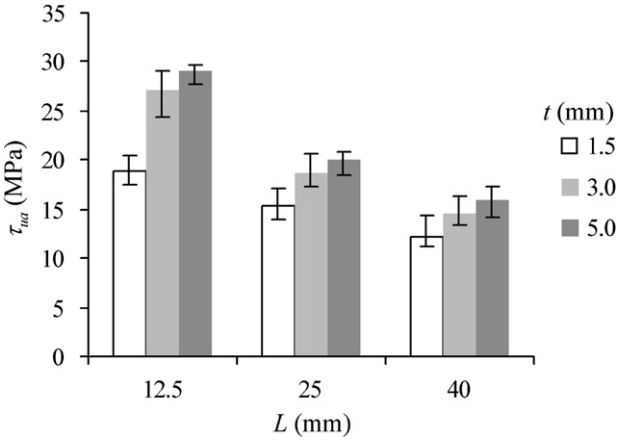

Fig. 5. Average and scatter interval of apparent strengths measured for AS SLJ without spew fillets.

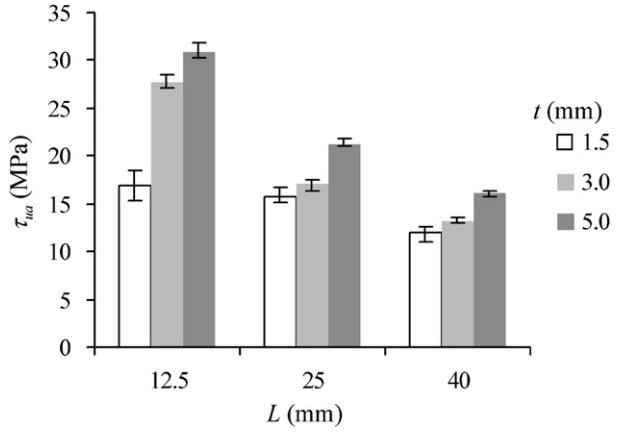

Fig. 6. Average and scatter interval of apparent strengths measured for L3450 SLJ with spew fillets.

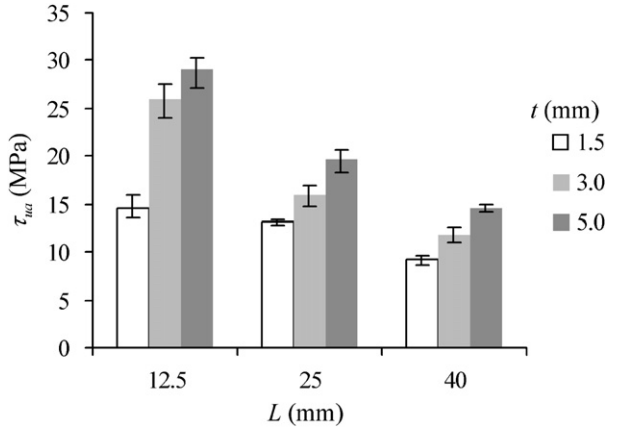

Fig. 7. Average and scatter interval of apparent strengths measured for L3450 SLJ without spew fillets.

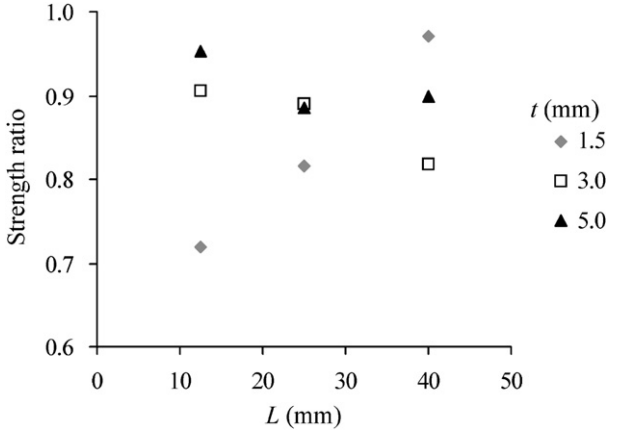

Fig. 8. No fillet-to-fillet apparent strength ratio of AS SLJ.

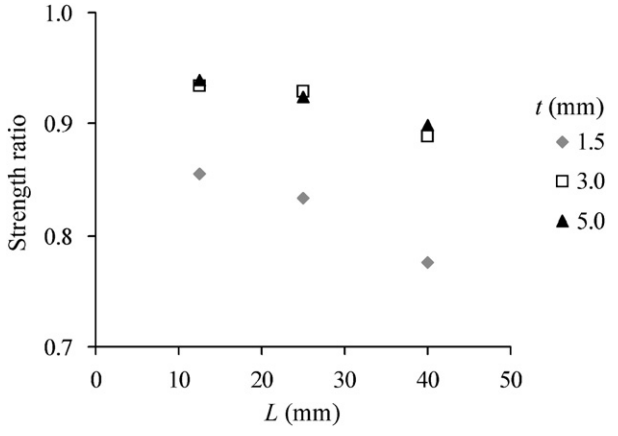

Fig. 9. No fillet-to-fillet apparent strength ratio of L3450 SLJ.

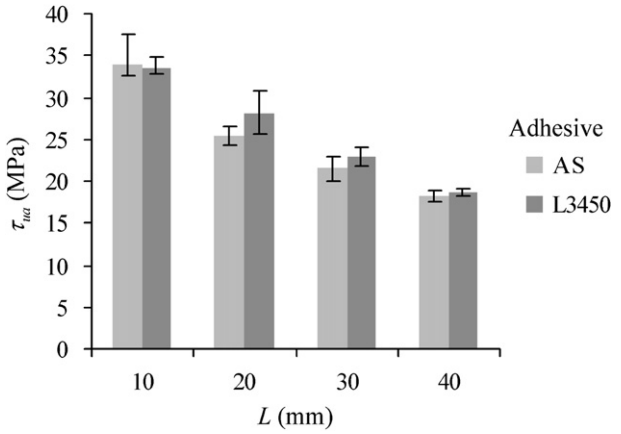

Fig. 10. Average and scatter interval of apparent strengths measured in TAS tests.

spew fillets. AS SLJ (1.5, L) joints were the exception to this behaviour because of extensive adherend plastic deformations.

Results obtained in TAS tests (Fig. 10) can be interpreted similarly i.e. longer overlaps give rise to higher stress concentration and thus to lower τ_{ua} values. Therefore, the present results confirm that failure is dictated by high stresses at joint ends. However, a failure criterion can only be determined through numerical analyses.

3. Analysis

3.1. Modelling approach

As seen in Section 1, one of the main problems in FE modelling of adhesive joints is the adhesive/adherend interface singularity for the straight edge geometry. Local stresses or strains thus depend significantly on the level of mesh refinement, especially close to the interface. Therefore, a different approach was pursued, which is based on adopting a uniform through-thickness stress state for the adhesive layer. Obviously, this approach demands that the adhesive layer is thin, which is clearly the case of the joints analysed here. Moreover, it can be easily implemented in standard FE codes by selecting constant strain elements, such as the two-dimensional four-node reduced integration plane strain. These elements have the additional advantage of being well suited for problems involving large strain gradients and plastic deformations. Accordingly, models of SLJ and TAS tests were constructed with the commercial code ABAQUS® using CPE4R elements. It should be said that such elements were also appropriate to model adherends in regions and joint types where plastic deformations occurred. In other cases, incompatible mode elements would be more effective. Nevertheless, the present analyses were two-dimensional plane strain and thus refined meshes with CPE4R elements did not pose any computational cost problems. However, mesh visualisation requires high magnification zooming, as exemplified in Figs. 11 and 12. Models of BJT and NRS specimens were

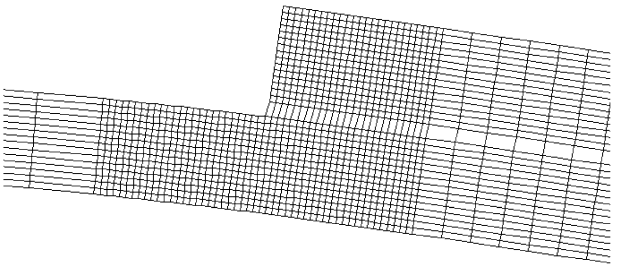

Fig. 11. FE mesh of a SLJ (1.5,25) in the deformed configuration: close-up view of the overlap area.

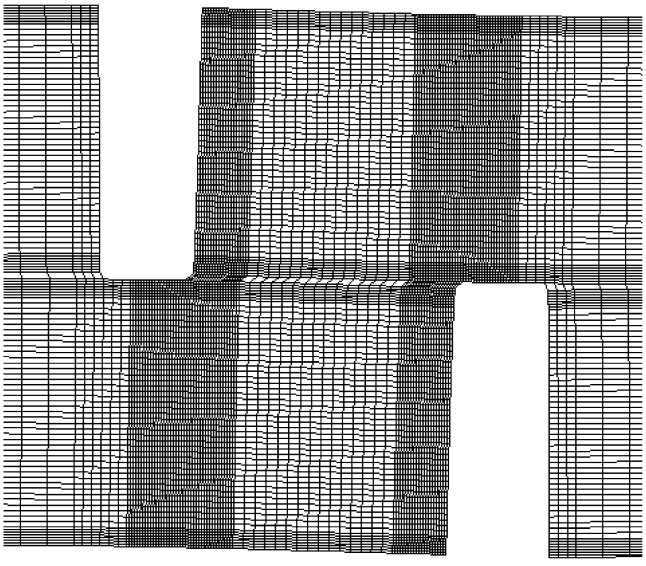

Fig. 12. FE mesh of a TAS joint: close-up view of the overlap area.

built with axysimmetric four-node reduced integration CAX4R and CGAX4R elements.

Preliminary mesh refinement studies showed that modelling the adhesive layer by a single row of constant strain elements gave accurate results for the global load-displacement behaviour of all joints. Differences relative to models with three rows of elements across the adhesive thickness were lower than 0.3%. Furthermore, the interface singularity created significant numerical difficulties in non-linear analyses with the latter models. Therefore, the approach followed here also has the significant practical advantage of minimising numerical problems. On the other hand, it was essential that the element size near joint ends was small enough to yield accurate local stresses and strains. Meshes were constructed with 0.2, 0.1 and 0.05 mm local element size. Maximum differences in results from the latter meshes were lower than 0.5%, thus showing an appropriate level of refinement had been reached.

Geometrically linear analyses were first performed assuming linear elastic isotropic behaviour for adherend and adhesive. The AISI 304 steel adherends have Young's modulus $E = 193$ GPa and Poisson $\nu = 0.3$ [15]. On the other hand, $E = 1.8$ GPa and $\nu = 0.38$ were used for both

Table 1
Adhesive strengths used in FE analyses

Case	β (deg.)	σ_{ut} (MPa)	τ_u (MPa)	σ_{uc} (MPa)
B45T	45.0	35.0	26.9	70.0
B45S	45.0	45.5	35.0	91.0
B56T	56.0	35.0	30.2	103.4
B56S	56.0	40.6	35.0	119.9
B65	65.5	35.0	35.0	225.6

adhesives considering manufacturers datasheets and the typical $\nu = 0.35$–0.41 range for epoxy resins. In a second stage, geometrical non-linearity and plasticity were introduced. The whole stress–strain curve of the AISI 304 steel was obtained from Refs. [15] and von Mises yielding was used. However, the complete stress-strain curves and the multiaxial yield criteria of the adhesives used in this study have not been determined. Therefore, elastic-perfect plasticity with Drucker–Prager [21] yielding was assumed. Relations between adhesive tensile (σ_{ut}), compressive (σ_{uc}) and shear (τ_u) strengths are

$$\frac{\sigma_{uc}}{\sigma_{ut}} = \frac{3+\tan\beta}{3-\tan\beta}, \quad \frac{\tau_u}{\sigma_{ut}} = \frac{3+\tan\beta}{3\sqrt{3}} \tag{1}$$

where β is the friction angle. As seen in Section 2.2, joint strength results suggested $\sigma_{ut} \approx \tau_u$ and thus $\beta = 65.5^\circ$. However, this results in $\sigma_{uc}/\sigma_{ut} = 6.5$, while the literature [22] and material databases give a typical 2–4 range for epoxies. This corresponds to $\beta = 45$–61° and to $\tau_u/\sigma_{ut} = 0.77$–$0.92$ intervals, and thus would imply that the above joint tests provided underestimates of σ_{ut} and/or overestimates of τ_u. In view of these uncertainties and the results of Fig. 3, simulations were performed for the cases of Table 1, which were defined by setting σ_{ut} or τ_u equal to 35 MPa and using $\beta = 45$, 56 and 65.5°.

Finally, it is important to highlight two important consequences of the present modelling approach on the subsequent analysis of experimental results. First, the elastic-perfectly plastic behaviour assumed for the adhesives requires strain based joint failure predictions. Second, owing to the through-thickness constant strain modelling, the ultimate strain may be a property of the adhesive or a property of the interface, depending on the nature of the failure mode.

3.2. Comparison with experimental data

Figs. 13–15 depict the maximum shear and peel stresses at SLJ and TAS joint ends in linear analyses. The qualitative explanation of experimental results given in Section 2.2 is clearly supported, although non-linear analyses are essential for identifying a joint failure criterion. First, however, attention was given to tests that could yield adhesive tensile and shear strengths.

As expected, non-linear simulations of BJT tests showed radial stresses of the same order of magnitude of

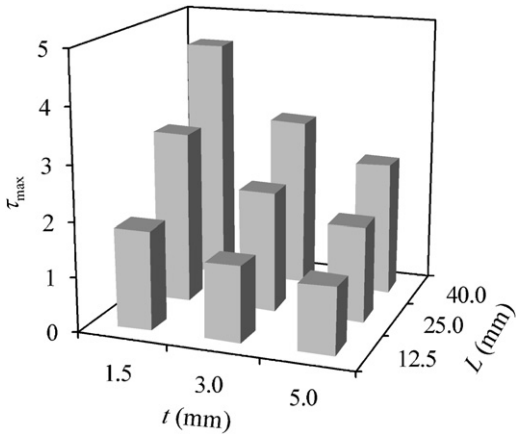

Fig. 13. Maximum shear stress at SLJ ends. Stress values were normalised by the overlap average shear stress.

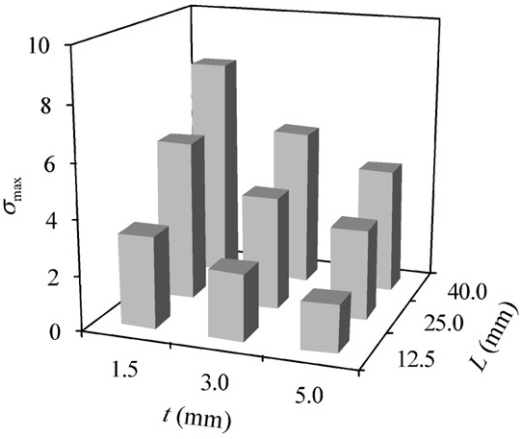

Fig. 14. Maximum peel stress at SLJ ends. Stress values were normalised by the overlap average shear stress.

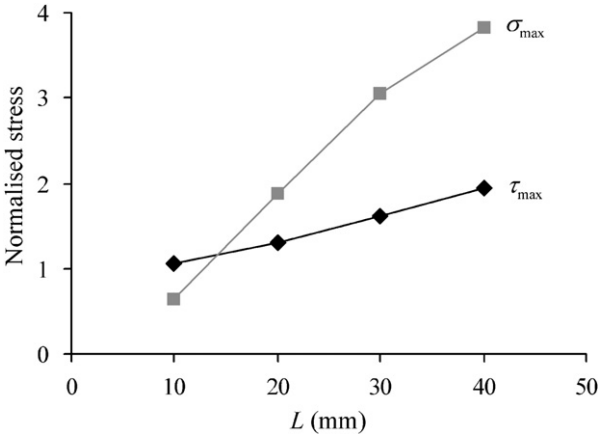

Fig. 15. Maximum shear and peel stresses at TAS joint ends. Stress values were normalised by the overlap average shear stress.

axial stresses, both quasi-uniformly distributed. In these circumstances, the true tensile strength may actually be overestimated for ductile adhesives with small β values

(Fig. 16). This could explain why BJT tests sometimes give higher strengths than tests on bulk specimens [23].

On the other hand, a pure shear stress state was obtained in the linear elastic analysis of the NRS test. However, adhesive plasticity gave rise to significant radial and axial stresses that could cause overestimation of the adhesive shear strength (Fig. 17), especially for ductile adhesives with high β values. As to TAS(10) tests, although the shear

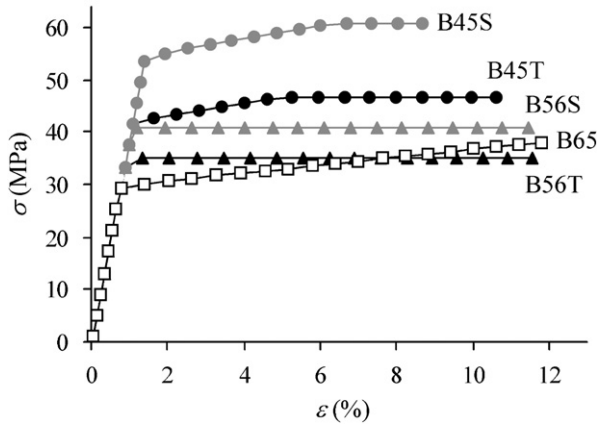

Fig. 16. Stress–strain curves obtained in FE analyses of BJT tests for the adhesive strengths of Table 1.

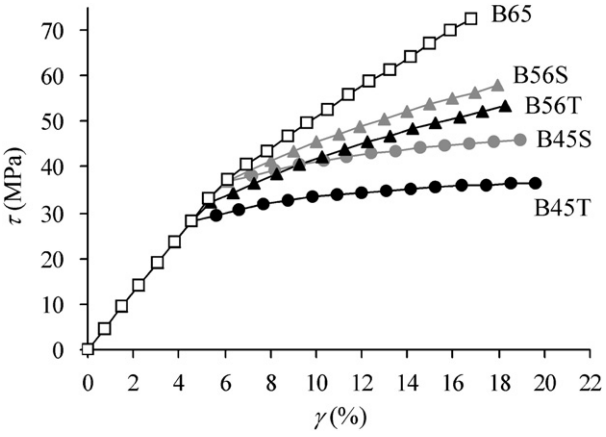

Fig. 17. Stress–strain curves obtained in FE analyses of NRS tests for the adhesive strengths of Table 1.

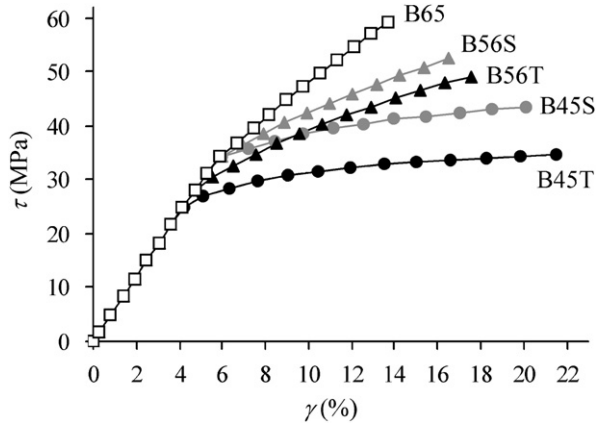

Fig. 18. Stress–strain curves obtained in FE analyses of TAS(10) joints for the adhesive strengths of Table 1.

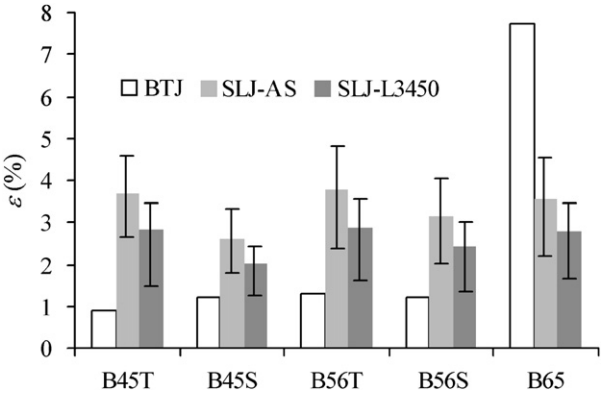

Fig. 19. Normal strains and maximum peel strains obtained in FE analyses of BTJ and SLJ tests. Adhesive strengths used are given in Table 1. Results for SLJ are depicted in the form of average and scatter interval for all geometries.

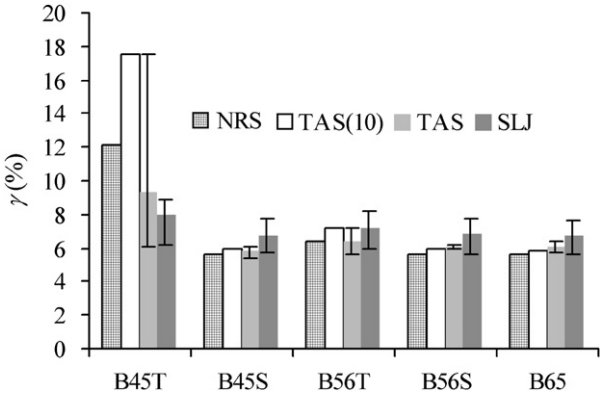

Fig. 20. Maximum shear strains obtained in FE analyses of NRS, TAS and SLJ tests. AS adhesive strengths used are given in Table 1. SLJ and TAS test results are depicted in the form of average and scatter interval for all geometries.

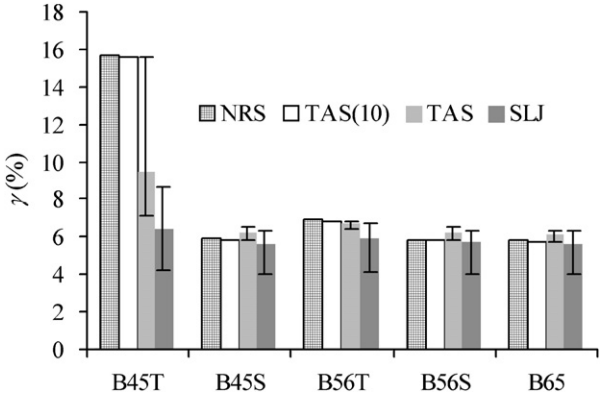

Fig. 21. Maximum shear strains obtained in FE analyses of NRS, TAS and SLJ tests. L3450 adhesive strengths used are given in Table 1. SLJ and TAS test results are depicted in the form of average and scatter interval for all geometries.

stress distribution along the overlap was practically uniform, significant peel stresses were present at the joint ends (Fig. 15). Again, the complex stress state can lead to a significant shear strength overestimation for ductile adhesives (Fig. 18). In fact, shear stress–strain curves of NRS and TAS(10) tests were similar, although the latter was more conservative.

Therefore, the above results raised important questions about the meaningfulness of strengths measured in BJT, NRS and TAS(10) tests. Furthermore, they reinforced the interest in analysing the cases defined in Table 1. Unfortunately, the combination of FE analyses with BJT test data does not allow an accurate estimation of the adhesive normal failure strain. This is essentially due to the elastic-perfectly plastic approximation adopted, which generates a plateau or a very low slope in stress–strain curves (Fig. 16). Nevertheless, Fig. 19 plots failure strains obtained from FE models of BJT tests using the strengths of Table 1. Calculated strains are quite low, a situation that is common in epoxy resins. The exception was the

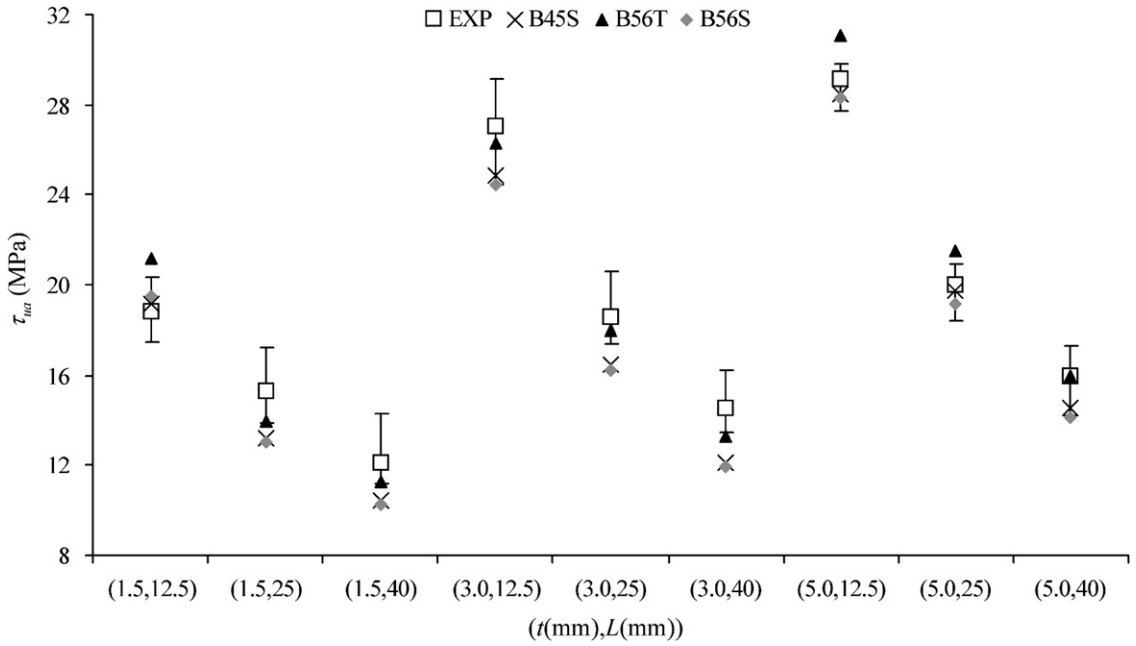

Fig. 22. Apparent strengths of AS SLJ: experimental (EXP) average and scatter interval and predictions using ultimate shear strains estimated from TAS(10) tests. Adhesive strengths used are given in Table 1.

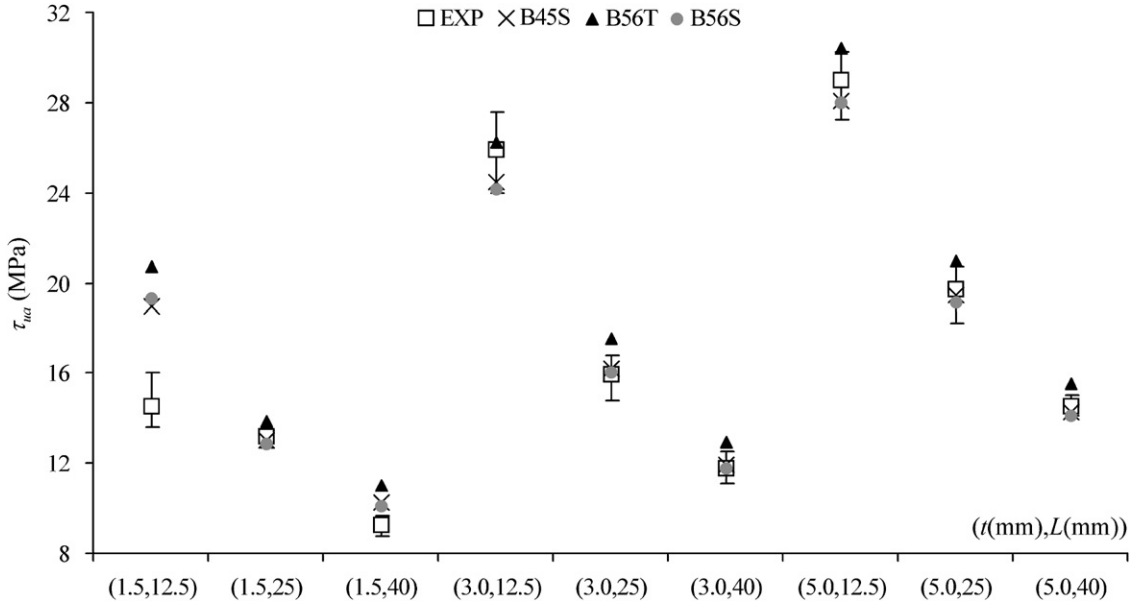

Fig. 23. Apparent strengths of L3450 SLJ: experimental (EXP) average and scatter interval and predictions using ultimate shear strains estimated from TAS(10) tests. Adhesive strengths used are given in Table 1.

$\beta = 65.5^{\circ}$ case, which predicted a relatively high failure strain. Since this material behaviour also implies very high compressive strengths, it is unlikely to be realistic for the adhesives used in this study. Fig. 19 also includes maximum peel strains at failure in SLJ computed from FE models using experimental failure loads. In spite of the uncertainties in this analysis, Fig. 19 suggests that maximum peel strains attained in SLJ are generally much higher than ultimate strains measured in tensile tests. This seems to be consistent with the existence of significant size effects, as peel stresses are highly localised. It can also be seen that maximum peel strains in SLJ varied significantly with geometry. Therefore, although the levels of strain localisation varied, it seems unlikely that failure was caused by excessive peel strains.

On the other hand, maximum shear strains at failure calculated for SLJ agreed reasonably well with those of TAS and NRS tests (Figs. 20 and 21). The exception was the B45T case (Table 1), which thus seems to be inadequate for the adhesives used. Moreover, apparent strengths of SLJ could generally be predicted with a fair degree of accuracy using ultimate shear strains estimated from TAS(10) tests (Figs. 22 and 23). In fact, prediction errors varied between -19.0% and 12.4%, a margin that can be considered satisfactory considering the scatter in experimental values and the uncertainties in adhesive strengths. In view of the failure modes observed, the ultimate shear strain measured in TAS(10) tests is an interface property of AS adhesive—AISI 304 steel joints, and a L3450 adhesive material property.

4. Conclusions

This paper reported an experimental and analytical study on the strength of stainless steel joints bonded with two epoxy adhesives. Napkin ring shear and 10 mm overlap length thick-adherend shear tests gave very similar shear strengths for both adhesives. Strengths measured in BJT tests were practically identical to shear strengths, a situation that some studies indicate to occur in polymers. However, subsequent finite element analyses suggested that strengths of ductile adhesives might be overestimated in the above tests. This is due to the complex stress state in joint tests and to pressure-dependent adhesive behaviour.

Other tests conducted were thick-adherend shear tests on joints with 20–40 mm overlap lengths and lap-shear tests on SLJs with 1.5–5.0-mm thick adherends and 12.5–40 mm overlap lengths. In both cases, the apparent strength (failure load divided by overlap area) decreased with the overlap length, although the failure load increased. On the other hand, the apparent strength of single-lap joints increased with adherend thickness. These trends correlated with the levels of stress concentration at joint ends obtained in linear FE analyses.

In order to identify a failure criterion, non-linear FE analyses were performed for all tests assuming adhesive Drucker–Prager yielding and a range of adhesive strengths that experimental results indicated to be realistic. Results suggested the adhesives could sustain highly localised peel stresses much higher than ultimate normal strains. Moreover, despite uncertainties on the true adhesive multi-axial stress–strain behaviour, the present FE analyses showed that joint failure could be fairly well predicted by a maximum shear strain criterion. The ultimate shear strain could be a material property of the adhesive or an interface property.

References

[1] Goland M, Reissner E. The stress in cemented joints. J Appl Mech 1944;66:A17.
[2] Hart-Smith LJ. In: Engineered materials handbook, vol. 3. ASM Int., 1987, p. 471.
[3] Adams RD, Comyn J, Wake WC. Structural adhesive joints in engineering. London: Chapman & Hall; 1997.
[4] Rispler AR, Tong L, Steven GP, Wisnom MR. Shape optimisation of adhesive fillets. Int J Adhes Adhes 2000;20:221.
[5] Li G, Lee-Sullivan P. Finite element and experimental studies on single-lap balanced joints in tension. Int J Adhes Adhes 2001;21:211.
[6] Wang CH, Rose LRF. Compact solutions for the corner singularity in bonded lap joints. Int J Adhes Adhes 2000;20:145.
[7] Towse A, Potter KD, Wisnom MR, Adams RD. The sensitivity of a Weibull failure criterion to singularity strength and local geometry variations. Int J Adhes Adhes 1999;19:71.
[8] Fernlund G, Papini M, McCammond D, Spelt JK. Fracture load predictions for adhesive joints. Compos Sci Technol 1994;51:587.
[9] Wahab MMA. On the use of fracture mechanics in designing a single lap adhesive joint. J Adhes Sci Technol 2000;14:851.
[10] Tvergaard V, Hutchinson JW. On the toughness of ductile adhesive joints. J Mech Phys Solids 1996;44:789.
[11] Yang QD, Thouless MD. Mixed-mode fracture analysis of plastically-deforming adhesive joints. Int J Fract 2001;110:175.
[12] Kafkalidis MS, Thouless MD. The effects of geometry and material properties on the fracture of single lap-shear joints. Int J Solids Struct 2002;39:4367.
[13] Campilho RDSG, de Moura MFSF, Domingues JJMS. Modelling single and double-lap repairs on composite materials. Compos Sci Technol 2005;65:1948.
[14] Pereira AB, de Morais AB. Strength of adhesively bonded stainless steel joints. Int J Adhes Adhes 2003;23:315.
[15] Rasmussen KJR. Full-range stress–strain curves for stainless steel alloys. Research report No R811. University of Sydney, 2001.
[16] ISO 11003-2:2001. Determination of shear behaviour of structural adhesives. Part 2: Tensile test method using thick adherends.
[17] Liu K, Piggott MR. Fracture failure processes in polymers. I: Mechanical tests and results. Polym Eng Sci 1998;38:60.
[18] Liu K, Piggott MR. Fracture failure processes in polymers. II: Fractographic evidence. Polym Eng Sci 1998;38:69.
[19] da Silva LFM, Adams RD. Measurement of the mechanical properties of structural adhesives in tension and shear over a wide range of temperatures. J Adhes Sci Technol 2005;19:105.
[20] Chai H. The observation of deformation and damage at the tip of cracks in adhesive bonds loaded in shear and assessment of a criterion for fracture. Int J Fract 1993;60:311.
[21] Drucker DC, Prager W. Soil mechanics and plastic analysis or limit design. Q Appl Math 1952;10:157.
[22] Nielsen LE. Mechanical properties of polymers and composites. New York: Marcel Decker; 1993.
[23] Ikegami K, Fujii T, Kagawoe H, Kyoguku H, Motoie K, Nohno K, et al. Benchmark tests on adhesive strengths in butt, single and double lap joints and double-cantilever beams. Int J Adhes Adhes 1996;16:219.